

1 **Electrical conductivity of anhydrous and hydrous gabbroic melt**  
2 **under high temperature and high pressure: Implications for the**  
3 **high conductivity anomalies in the region of mid-ocean ridge**

4 Mengqi Wang<sup>1,2</sup>, Lidong Dai<sup>1\*</sup>, Haiying Hu<sup>1\*</sup>, Ziming Hu<sup>1,2</sup>, Chenxin Jing<sup>1,2</sup>, Chuanyu  
5 Yin<sup>1,2</sup>, Song Luo<sup>1,2</sup> and Jinhua Lai<sup>1,2</sup>

6 *<sup>1</sup>Key Laboratory of High-temperature and High-pressure Study of the Earth's Interior,*  
7 *Institute of Geochemistry, Chinese Academy of Sciences, Guiyang, China*

8 *<sup>2</sup>University of Chinese Academy of Sciences, Beijing, China*

9 To be submitted to ***Solid Earth***

10 February 26<sup>th</sup>, 2023

\*Authors to whom correspondence should be addressed: dailidong@vip.gyig.ac.cn and huhaiying@vip.gyig.ac.cn

## Abstract

11  
12 The electrical conductivity of gabbroic melt with four different water contents  
13 (i.e. 0, 2.59 wt%, 5.92 wt% and 8.32 wt%) was measured at temperatures of 873–  
14 1373 K and pressures of 1.0–3.0 GPa using YJ–3000t multi–anvil high–pressure  
15 apparatus and Solartron–1260 impedance spectroscopy analyzer. At a fixed water  
16 content of 2.59 wt%, the electrical conductivity of the sample slightly decreased with  
17 increasing pressure at the temperature range of 873–1373 K, and its corresponding  
18 activation energy and activation volume were determined as  $0.87 \pm 0.04$  eV and  $-1.98$   
19  $\pm 0.02$  cm<sup>3</sup> mole<sup>-1</sup>, respectively. Under the certain conditions of 873–1373 K and 1.0  
20 GPa, the electrical conductivity of the gabbroic melts tends to gradually increase as  
21 the rise of water content from 0 to 8.32 wt%, and the activation enthalpy decreases  
22 from 0.93 eV to 0.63 eV, accordingly. Furthermore, the functional relation models for  
23 the electrical conductivity of gabbroic melts with the variations of temperature,  
24 pressure and water content were constructed at high–temperature and high–pressure  
25 conditions, respectively. In addition, the dependence relation of the electrical  
26 conductivity of melts with the degree of depolymerization was explored under  
27 conditions of four different water contents, 1373 K and 1.0 GPa, and three previously  
28 available reported results on those of representative calc–alkaline igneous rock melts  
29 (i.e. dacitic melt, basaltic melt and andesitic melt) were detailedly compared. In  
30 comprehensive combination with our presently acquired electrical conductivity data  
31 of gabbroic melt with four different water contents and the available data of  
32 polycrystalline olivine, the electrical conductivity of gabbroic melt–olivine system on

33 the variation of volume percentage of anhydrous and hydrous melts was successfully  
34 constructed by virtue of the typical Hashin–Shtrikman upper bound model. In light of  
35 the electrical conductivity of gabbroic melt–olivine system with the previous MT  
36 results, we find that the anhydrous and hydrous gabbroic melts can be employed to  
37 reasonably interpret the high conductivity anomalies in the Mohns ridge of the Arctic  
38 Ocean.

39 **Keywords: electrical conductivity, gabbroic melt, degree of depolymerization,**  
40 **high conductivity anomalies, Mohns ridge**

## 41 1 Introduction

42 The hydrous melt for various rocks and minerals widely exists at active plate  
43 tectonic boundaries such as mid-ocean ridge, subduction zone, orogenic belt, etc.  
44 (Shen and Forsyth, 1995; White et al., 2001; Wallace, 2005; Wu et al., 2018; Sim et  
45 al., 2020; Förster and Selway, 2021; Li et al., 2022; Turner and Langmuir, 2022). For  
46 the typical Mohns ridge in the Arctic Ocean, there existed a large amount of high  
47 conductivity anomaly phenomena with its correspondent magnitude of 0.08–0.32 S  
48  $\text{m}^{-1}$  for the gabbro-rich regions have been revealed on the basis of previous  
49 magnetotelluric (MT) controlled source electromagnetic (CSEM) results (Johansen et  
50 al., 2019).

51 Previously available researches have indicated that gabbroic and basaltic melts  
52 contain a large amount of water, and the water content for the certain type of melt  
53 may be discrepant within the different depth ranges of the oceanic crust (Dixon et al.,  
54 1995; Almeev et al., 2008; Shaw et al., 2010; Leuthold et al., 2018). Meanwhile,  
55 water content is also considered as a crucial ingredient to possibly affect the electrical  
56 conductivity of melt, and there are a large number of previously available reported  
57 results for the variation of water content on the electrical conductivity of some  
58 representative calc-alkaline igneous rock melts at high temperature and high pressure  
59 in the recently several years (Ni et al., 2011; Laumonier et al., 2015; Guo et al., 2017;  
60 Chen et al., 2018). For example, Ni et al. (2011) measured the electrical conductivity  
61 of hydrous basaltic melt within water content range of 0–6.3 wt% at conditions of  
62 1473–1923 K and 2.0 GPa, and they found that the electrical conductivity of basaltic

63 melt with a fixed water content of 6.3 wt% was of the rough 1.0 order of magnitude  
64 higher than that of the anhydrous sample. The electrical conductivity of dacitic melt  
65 within the water content range of 0–12 wt% was systematically investigated by  
66 Laumonier et al. (2015) within temperature range of 673–1623 K and pressures of  
67 0.3–3.0 GPa. As pointed out by Laumonier et al. (2015), the high conductivity  
68 anomalies in the Uturuncu Volcano could be explained by the presence of hydrous  
69 dacitic melt. By virtue of a piston cylinder high–pressure apparatus and sweeping–  
70 frequency impedance spectroscopy, Guo et al. (2017) obtained the electrical  
71 conductivity data of andesitic melt within the water content range of 0.01–5.90 wt% at  
72 conditions of 1164–1573 K and 0.5–1.0 GPa. Their experimental results indicated that  
73 the presence of less than 20 vol% of hydrous andesitic melt within the water content  
74 range of 6–9 wt% can be used to interpret the high conductivity anomalies beneath the  
75 surface of the Uturuncu Volcano. Electrical conductivity measurements of the  
76 hydrous leucogranitic melt by Chen et al. (2018) at conditions of 739–1680 K and  
77 0.36–2.52 GPa were systematically carried out within the water content range of  
78 2.73–11.97 wt%. In comprehensive combination with previous magnetotelluric data  
79 in the northwest Himalaya, they considered that water–rich leucogranitic melts with a  
80 volume percentage range of 4–16 vol% can be applied to reasonably explain the high  
81 conductivity anomalies in these regions.

82 For the natural gabbroic rock, some previously available electrical conductivity  
83 results were obtained using the piston–cylinder and multi–anvil high–pressure  
84 apparatus at high temperature and high pressure. Sato and Ida (1984) measured the

85 electrical conductivity of the olivine–gabbro containing gabbroic melt at the  
86 temperature range from 1123 K to 1473 K and atmospheric pressure, and the effects  
87 of ionic diffusion of charge carriers (i.e. sodium, iron, magnesium and/or calcium ions)  
88 and geometric structure of melt on the electrical conductivity of olivine–gabbro  
89 samples were detailedly explored. The measurements of electrical conductivity for  
90 natural gabbro were carried out at conditions of 1023–1423 K and room pressure by  
91 Schilling et al. (1997), and they proposed that the electrical conductivity of samples  
92 can be enhanced by the increasing volume percentage of gabbroic melt. As for the  
93 natural Oman gabbro, the electrical conductivity of gabbroic melt with the volume  
94 percentage proportion of 34 % was ~1.0–2.0 orders of magnitude higher than that of  
95 melt–free sample within the temperature range from 1073 K to 1523 K and pressures  
96 of 0.3–1.0 GPa (Maumus et al., 2005). However, the influence of water content on the  
97 electrical conductivity of gabbroic melt at high temperature and high pressure was not  
98 investigated in detail. Consequently, it is crucial to make a systematic investigation on  
99 the electrical conductivity of gabbroic melt with different water contents at high–  
100 temperature and high–pressure conditions.

101 In the present studies, a series of electrical conductivity on the gabbroic melts  
102 were systematically performed under conditions of 873–1373 K, 1.0–3.0 GPa and the  
103 variation of water content range from 0 to 8.32 wt%. The effects of temperature,  
104 pressure and water content on the electrical conductivity of gabbroic melt are deeply  
105 explored, and the functional relation models have been successfully established at  
106 high–temperature and high–pressure conditions. In conjunction with the degree of

107 depolymerization, the electrical conductivity of gabbroic melt with different water  
108 contents is compared with that of three representative calc–alkaline igneous rock  
109 melts (i.e. dacitic melt, andesitic melt and basaltic melt). Based on the calculated  
110 electrical conductivity of gabbroic melt–olivine system, its potential geophysical  
111 implication was detailedly discussed in the Mohns ridge of the Arctic Ocean.

## 112 **2 Experimental procedures**

### 113 **2.1 Sample Preparation**

114 The natural gabbroic rock used in this study was collected from the ophiolite  
115 suite in the region of Ganzi Tibetan autonomous prefecture, Sichuan province, China.  
116 By virtue of the high–temperature quenched melt for the natural rock powder, the  
117 anhydrous and hydrous gabbroic melts are successfully obtained. Firstly, the fresh  
118 natural gabbro was finely crushed and ground into the sample powder with the grain  
119 size of less than 50  $\mu\text{m}$  in an agate mortar. Then, the sample powder was kept in the  
120 furnace at 473 K to remove the absorbed water. To obtain the homogeneously initial  
121 materials for the subsequent electrical conductivity measurement, the powder of  
122 gabbroic rock was melted at the temperature of 1473 K for 1.5 hours and rapidly  
123 quenched in a high–temperature muffle furnace. Further, gabbroic melt was crushed  
124 and ground again into powder with a grain size less than 50  $\mu\text{m}$  and stored in a  
125 vacuum dry furnace at 373 K. To synthesize the hydrous gabbroic melt, the desired  
126 amount of deionized water was added to the powder, and subsequently, the sample  
127 encapsulated in a gold tube using the Lampert–Puk precise welding device. After that,  
128 the starting hydrous gabbroic melts with different water contents were synthesized at

129 conditions of 1373 K and 1.0–3.0 GPa for 12 hours in the YJ–3000t multi–anvil  
130 high–pressure apparatus, and all of these obtained samples are homogeneous without  
131 any available crystals or bubbles. Detailed hot–pressed sintering assemblage was  
132 similar to that previously described by Hu et al. (2022a). Lastly, all of the gabbroic  
133 melts were polished into cylinders with diameters of ~4.0–5.0 mm and heights of  
134 ~4.0–6.0 mm, and kept in muffle furnace at 423 K for 10 hours to eliminate the  
135 absorbed water for subsequent electrical conductivity measurements. The chemical  
136 compositions of anhydrous and hydrous gabbroic melts were analyzed by virtue of the  
137 electronic probe microscopy analysis (EPMA) at the State Key Laboratory of Ore  
138 Deposit Geochemistry, Institute of Geochemistry, Chinese Academy of Sciences,  
139 Guiyang, China, as shown in Table 1.

## 140 **2.2 High–pressure cell and impedance measurements**

141 High–pressure complex impedance measurements for gabbroic melt were  
142 performed by using Solartron–1260 impedance spectroscopy analyzer in the YJ–3000t  
143 multi–anvil high–pressure apparatus. The cross–section diagram of sample assembly  
144 for electrical conductivity measurements was shown in Fig. 1. Before high–pressure  
145 cell was assembled, the cubic pressure medium of pyrophyllite with dimension of  
146  $32.5 \times 32.5 \times 32.5 \text{ mm}^3$  and insulation sleeves were baked at 1073 K in a muffle furnace  
147 for 5 hours to remove the absorbed water. The sample was placed at the middle of the  
148 alumina and magnesia insulation sleeves, and sandwiched with two symmetric nickel  
149 electrodes. The electrode was connected with a  $\text{Ni}_{97}\text{Al}_3$  wire to a Solartron–1260  
150 impedance spectroscopy analyzer. To shield against external electromagnetism and



151 spurious signal interference, the nickel foil with a thickness of 0.025 mm was installed  
152 between the alumina and magnesia sleeves, and linked to the Earth line. Three-layer  
153 stainless steel sheets with a total thickness of 0.5 mm were adopted as the heater,  
154 which were installed between the cubic pressure medium of pyrophyllite and alumina  
155 sleeve. After that, the sample assembly was stored in the vacuum dry furnace at 423 K  
156 for at least 12 hours before the electrical conductivity measurements.

157       During the experiment, the pressure was slowly raised with a rate of 1.0 GPa h<sup>-1</sup>  
158 until it reached the desired value, and then the temperature was gradually increased  
159 with a speed of 5.0 K min<sup>-1</sup>. Under predesignated high-temperature and high-  
160 pressure condition, impedance spectra of samples were collected in the frequency  
161 range of 10<sup>0</sup>–10<sup>6</sup> Hz and the applied signal voltage of 1.0 V. To obtain reproducible  
162 data, impedance spectra of samples were measured at least two continuously heating-  
163 cooling cycles under conditions of 873–1373 K and 1.0–3.0 GPa. The uncertainties of  
164 temperature and pressure were less than 5.0 K and 0.1 GPa, respectively. The detailed  
165 experimental principles and measurement procedures were described by Dai et al.  
166 (2008) and Hu et al. (2022b).

### 167 **2.3 Determination of the water content**

168       The water content of gabbroic melt before and after the electrical conductivity  
169 measurements was performed by virtue of the Vertex-70V and Hyperion-1000  
170 vacuum Fourier transform infrared (FT-IR) spectroscopy analyzer. The samples were  
171 double-polished up to a thickness of ~50 μm. At least five spectra were conducted on  
172 the different regions of transparent sample surfaces and made an average value in

173 order to avoid the heterogeneity effect of water distribution. A detailed experimental  
174 method and procedure for the FT–IR measurement was detailedly presented by Hong  
175 et al. (2022) and Hu et al. (2022b). For the hydrous gabbroic melts, the signal of the  
176 fundamental stretching H<sub>2</sub>O vibrational spectroscopy at the peak position of ~3530  
177 cm<sup>-1</sup> of hydroxyl band revealed to be oversaturated, which was similar to the  
178 previously obtained results on hydrous dacitic melts reported by Laumonier et al.  
179 (2015). The absorbance of gabbroic melt in the water-bearing FTIR spectroscopy at  
180 the wavenumber of ~3530 cm<sup>-1</sup> band is possibly related to the charge carrier species  
181 of hydrogen-related defects, such as hydroxyl (OH), free proton et al., which was  
182 similar to previously reported hydrous electrical conductivity results on many  
183 nominally anhydrous minerals (Huang et al., 2005; Dai and Karato, 2009a, 2014a;  
184 2020). For water-rich samples, two obviously characteristic peaks were appeared at  
185 the correspondent wavenumbers of ~4500 cm<sup>-1</sup> and ~5200 cm<sup>-1</sup>, which were  
186 representing the hydroxyl band and molecular water band with an available  
187 over-saturated state for gabbroic melts, respectively (Stolper, 1982; Dixon et al., 1995;  
188 Guo et al., 2017). Thus, we make the integration at the wavenumber ranges of 3000–  
189 4000 cm<sup>-1</sup> and 4000–5800 cm<sup>-1</sup> for the anhydrous and hydrous samples to precisely  
190 determine the water content of gabbroic melts, respectively. The typical FT–IR  
191 spectra of gabbroic melt within the wavenumbers range of 2500–5800 cm<sup>-1</sup> are shown  
192 in Fig. 2. The water content of gabbroic melt ( $C_{\text{melt}}$ ) can be worked out by Beer–  
193 Lambert law,

$$194 \quad C = \omega A / \epsilon p d \quad (1)$$

195 
$$C_{\text{melt}} = C_{\text{OH}} + C_{\text{H}_2\text{O}} \quad (2)$$

196 In here, the signal of  $\omega$  stands for the molar mass of  $\text{H}_2\text{O}$  ( $18.02 \text{ g mole}^{-1}$ ),  $A$  stands  
197 for the integrated area of absorption spectra ( $\text{cm}^{-2}$ ),  $\rho$  stands for the density ( $\text{g cm}^{-3}$ ),  $d$   
198 stands for the thickness of thin section (cm), and  $\varepsilon$  stands for the integral molar  
199 absorption coefficient ( $\text{L mole}^{-1} \cdot \text{cm}^{-2}$ ). As presented the calculated melt density  
200 method by Luhr (2001), our density of gabbroic melt is determined as  $2.764 \times 10^3 \text{ g L}^{-1}$ .  
201 Molar absorption coefficients of  $\varepsilon_{\text{OH}}$  and  $\varepsilon_{\text{H}_2\text{O}}$  were adopted from Dixon et al.  
202 (1995). According to the Eqs. 1 and 2, the water contents for three obtained hydrous  
203 gabbroic melts were calculated as 2.59 wt%, 5.92 wt% and 8.32 wt% at the  
204 wavenumber range from  $4000 \text{ cm}^{-1}$  to  $5800 \text{ cm}^{-1}$ , respectively. From Figure 2, it is  
205 clear that the absorbance absorption of gabbroic melts in the water-rich FTIR  
206 spectroscopy at the wavenumber of  $\sim 3530 \text{ cm}^{-1}$  band spanning a wide range of water  
207 contents look identical. Obviously, the intensity of FT-IR spectra will decrease from  
208 water-rich (i.e. its correspondent water content is higher than 2.59 wt%) to water-poor  
209 (i.e. anhydrous) gabbroic melts. As displayed in Table 2, there is no significant loss of  
210 water for hydrous gabbroic melt during the electrical conductivity experiment. At the  
211 same time, the corresponding error bars of each water contents for the initial and  
212 recovered gabbroic melts are detailedly included in Table 2.

### 213 **3 RESULTS**

214 In the present experiments, the electrical conductivity of gabbroic melt with four  
215 different water contents (i.e. 0, 2.59 wt%, 5.92 wt% and 8.32 wt%) was measured at  
216 temperature range of 873–1373 K and pressures of 1.0–3.0 GPa. The representative

217 complex impedance spectra of gabbroic melt with the 2.59 wt% water at conditions of  
 218 873–1373 K and 2.0 GPa were shown in Fig. 3. According to the theory of AC  
 219 complex impedance spectra, the impedance spectra of gabbroic melts within the  
 220 high-frequency range from  $\sim 10^2$ – $10^3$  Hz to  $10^6$  Hz can be interpreted as the bulk  
 221 conduction mechanism (i.e. grain interior), and whereas, the impedance spectra of  
 222 sample within the low-frequency range from  $10^0$  Hz to  $\sim 10^2$ – $10^3$  Hz represent the  
 223 grain boundary conduction mechanism or the polarization process at sample–electrode  
 224 interface (Tyburczy and Roberts (1990), Dai et al. (2008, 2012, 2013, 2014, 2016);  
 225 Dai and Karato (2009a, b, c, 2020)). And thus, a series connection of  $R_S$ – $CPE_S$  ( $R_S$   
 226 and  $CPE_S$  represent the resistance and constant–phase element of the gabbroic melt,  
 227 respectively) and  $R_E$ – $CPE_E$  ( $R_E$  and  $CPE_E$  represent the interface resistance and  
 228 constant–phase element for electrode effect, respectively) were employed as the  
 229 equivalent circuit within a relatively lower temperature range of 873–1123 K. As far  
 230 as the higher temperature ranges of 1173–1373 K, the equivalent circuit was consisted  
 231 of the series connection of one resistance and one parallel resistance with the constant  
 232 phase element (CPE). The electrical conductivity of sample can be calculated,

$$233 \quad \sigma = L/SR \quad (3)$$

234 In here,  $L$ ,  $S$  and  $R$  stand for the length of sample (m), the cross–section area of  
 235 electrode ( $m^2$ ) and the electrical resistance of sample ( $\Omega$ ), respectively. And the  
 236 electrical conductivity of gabbroic melt and temperatures conformed to the Arrhenius  
 237 relation,

$$238 \quad \sigma = \sigma_0 \exp(-\Delta H/kT) \quad (4)$$

239 In here,  $\sigma_0$  stands for the pre-exponential factor ( $\text{S m}^{-1}$ ),  $k$  stands for the Boltzmann  
240 constant ( $\text{eV K}^{-1}$ ), and  $T$  stands for the absolute temperature (K), respectively. All of  
241 these fitted parameters for the electrical conductivity of anhydrous and hydrous  
242 gabbroic melt under conditions of 873–1373 K and 1.0–3.0 GPa were listed in Table  
243 2.

244 For the gabbroic melt with a fixed water content of 2.59 wt%, the electrical  
245 conductivity results for two continuously heating-cooling cycles at 873–1373 K and  
246 3.0 GPa were shown in Fig. 4. In the first heating cycle within the temperature range  
247 of 923–1073 K, the electrical conductivity of sample was slightly deviated with those  
248 of subsequent results in the first cooling and second heating-cooling cycles. Whereas,  
249 the deviation degree became more and more small and finally overlapped at much  
250 higher temperature range of 1123–1373 K. As a whole, the electrical conductivity of  
251 sample was almost reproducible in the first cooling and second heating-cooling cycles.  
252 And therefore, the electrical conductivity results were acquired by virtue of fitting  
253 experimental data during the process of the first cooling and second heating-cooling  
254 cycles.

## 255 **4 Discussions**

### 256 **4.1 Influence of pressure on electrical conductivity**

257 To identify the effect of pressure on the electrical conductivity of sample, the  
258 electrical conductivity of hydrous gabbroic melt was acquired under condition of 873–  
259 1373 K, 1.0–3.0 GPa and a fixed water content of 2.59 wt%. As illustrated in Fig. 5,  
260 the electrical conductivity of sample and temperature conformed to the Arrhenius

261 relation at a certain water content and pressure condition. In the present studies, a  
 262 slightly negative dependence relation for the electrical conductivity of hydrous  
 263 gabbroic melt with a fixed water content of 2.59 wt% on the pressure was observed.  
 264 The electrical conductivity of sample slightly decreases by around 1.6 times at as  
 265 pressure enhances from 1.0 GPa to 3.0 GPa at temperature range of 873–1373 K.  
 266 Accordingly, the pre-exponential factor reduces from  $3.02 \times 10^3 \text{ S m}^{-1}$  to  $6.17 \times 10^2 \text{ S}$   
 267  $\text{m}^{-1}$ , and the activation enthalpy value decreases from 0.85 eV to 0.81 eV,  
 268 respectively.

269 Furthermore, the influence of pressure on the electrical conductivity of gabbroic  
 270 melt can be depicted as,

$$271 \quad \sigma = A_0(1-BP) \cdot \exp\left[-\frac{\Delta U + P\Delta V}{kT}\right] \quad (5)$$

272 In here, the pre-exponential factor ( $\sigma_0$ ) and activation enthalpy ( $\Delta H$ ) of pressure  
 273 dependence can be illustrated as the relations of  $\sigma_0 = A_0(1-BP)$  and  $\Delta H = \Delta U + P\Delta V$ .  
 274 All of the listed parameters including  $\Delta U$ ,  $\Delta V$ , and  $P$  stand for the activation energy  
 275 (eV), the activation volume ( $\text{cm}^3 \text{ mole}^{-1}$ ) and pressure (GPa), and as well as  $B$  is  
 276 representing a constant, respectively. Furthermore, the electrical conductivity of  
 277 gabbroic melt along with the variations of temperature, pressure and water content is  
 278 fitted accordingly and the detailed fitting results are displayed in Table 3. The  
 279 logarithmic electrical conductivity of gabbroic melt with a fixed water content of 2.59  
 280 wt% and the inverse temperature follows a good linear relation, which reveals only  
 281 one main conduction mechanism operating the electrical transport within our  
 282 experimental temperature and pressure ranges. By virtue of the available pressure–

283 dependent electrical conductivity, we also can extrapolate the relationship between the  
284 electrical conductivity of gabbroic melt with a fixed water content of 2.59 wt% and  
285 temperature at atmospheric pressure. And then the pre-exponential factor and  
286 activation enthalpy at room pressure are calculated as  $5177 \text{ S m}^{-1}$  and  $0.87 \text{ eV}$ ,  
287 respectively. According to Eq. 5 and Table 3, the activation energy and activation  
288 volume of gabbroic melt with a fixed water content of 2.59 wt% can be determined as  
289  $0.87 \pm 0.04 \text{ eV}$  and  $-1.98 \pm 0.52 \text{ cm}^3 \text{ mole}^{-1}$ .

#### 290 **4.2 Influence of water content on electrical conductivity**

291 For a fixed pressure of 1.0 GPa, the influence of water content on the electrical  
292 conductivity of gabbroic melt at temperature range of 873–1373 K is detailedly shown  
293 in Fig. 6. The electrical conductivity of gabbroic melt with four different water  
294 contents gradually increases with the rise of temperature. For each correspondent  
295 water content (i.e. 0, 2.59 wt%, 5.92 wt% and 8.32 wt%), the logarithm of electrical  
296 conductivity of the sample and reciprocal temperature follows a good linear relation.  
297 On the other hand, when water content of gabbroic melt enhances from 0 to 8.32 wt%,  
298 the electrical conductivity of gabbroic melts tends to visibly increase, and whereas the  
299 activation enthalpy gradually reduces from 0.93 eV to 0.63 eV, accordingly. In short,  
300 our presently acquired electrical conductivity results show a substantial enhancement  
301 of water on the electrical conductivity of gabbroic melt, which are also observed  
302 among the electrical conductivity of other representative calc-alkaline igneous rock  
303 melts in the recent years (Ni et al., 2011; Laumonier et al., 2015; Guo et al., 2017;  
304 Chen et al., 2018).

305 The electrical conductivity of hydrous gabbroic melt can be expressed in terms  
306 of the charge species concentration dependence of the pre-exponential factor ( $A$ ),  
307 which behaves in an Arrhenius relation,

$$308 \quad \sigma = (A_1 + A_2 \cdot C_w^r) \cdot \exp\left(\frac{-\Delta H_0 - \alpha C_w^\beta}{RT}\right) \quad (6)$$

309 In here,  $C_w$  is water content of the sample (wt%),  $\Delta H_0$  stands for the activation  
310 enthalpy, and  $\alpha$ ,  $\beta$  and  $r$  stand for empirical power-law constants. By a non-linear  
311 global least-squares method, the electrical conductivity of gabbroic melt with  
312 different water contents was fitted and the fitted parameter results were listed in Table  
313 4. For the magnitude of water-dependent relation of  $r$  ( $0.43 \pm 0.05$ ), it makes clear  
314 that the water can dramatically enhance the electrical conductivity of gabbroic melt at  
315 conditions of 873–1373 K and 1.0 GPa.

### 316 **4.3 Comparisons with previous studies**

317 As displayed in Fig. 7, five previously reported results on the electrical  
318 conductivity of natural gabbro samples were employed to compare with our  
319 absolutely new results for the electrical conductivity of gabbroic melt (Sato and Ida,  
320 1984; Schilling et al., 1997; Maumus et al., 2005; Dai et al., 2015; Saito and  
321 Bagdassarov, 2018). As a whole, our acquired electrical conductivity results on  
322 gabbroic melts are obviously higher than those of natural gabbro at temperature range  
323 of 873–1373 K and pressure of 1.0 GPa. Both Sato and Ida (1984) and Schilling et al.  
324 (1997) have already performed the electrical conductivity measurements on natural  
325 gabbro at high temperature and atmospheric pressure. In case of the occurrence of  
326 temperature-induced partial melting, the electrical conductivity of sample will be



327 increased rapidly by several orders of magnitude. However, we find that there is no  
328 any relevant information on the water content for their previously reported electrical  
329 conductivity results on those of listed melting-bearing natural gabbro samples. The  
330 electrical conductivity results of natural gabbro containing 34 vol% melt from  
331 Maumus et al. (2005) are much lower than those of our present gabbroic melt, and the  
332 obvious discrepancy is possibly caused from the differentiation of the chemical  
333 composition and water content of gabbroic melt. In comparison with Saito and  
334 Bagdassarov (2018), there is a jump of three orders of magnitude in the electrical  
335 conductivity of sample, which is possibly originated from a relatively larger influence  
336 of melt volume percentage. As far as the previously reported electrical conductivity of  
337 natural gabbro with a relatively lower water content of ~610 ppm and free of any melt  
338 by Dai et al. (2015) at pressures of 0.5–2.0 GPa, there is an approximate electrical  
339 conductivity result on the anhydrous gabbroic melt to be observed in the present  
340 studies. And however, the dependence of electrical conductivity of anhydrous and  
341 hydrous gabbroic melts on the temperature, pressure and water content is still scarce  
342 under high-temperature and high-pressure conditions until now.

343 It is well known that the gabbroic melt is belonging to one type of representative  
344 calc-alkaline igneous rock. As usual, previously available conductivity results  
345 confirmed that the electrical conductivity of calc-alkaline igneous rock melts (i.e.  
346 dacitic melt, andesitic melt and basaltic melt) is also highly sensitive to the influential  
347 factor of the degree of depolymerization at high temperature and high pressure (Ni et  
348 al., 2011; Laumonier et al., 2015; Guo et al., 2017). The degree of depolymerization

349 can be characterized by the ratio of non-bridging oxygen ions per tetrahedrally  
350 coordinated cation (NBO/T). As pointed out by Mysen et al. (1982), the magnitude of  
351 degree of depolymerization on gabbroic melt can be worked out by our above-  
352 mentioned EPMA results in Table 1. And the dependence relation of electrical  
353 conductivity of gabbroic melts and degree of depolymerization was clearly displayed  
354 in Fig. 8 under conditions of four different water contents (i.e. 0, 2.59 wt%, 5.92 wt%  
355 and 8.32 wt%), 1373 K and 1.0 GPa. Under constant degree of depolymerization, it  
356 makes clear that a relatively lower electrical conductivity is observed in the  
357 anhydrous gabbroic melt under condition of 1373 K and 1.0 GPa. With the rise of  
358 water content, the electrical conductivity of gabbroic melts dramatically increases,  
359 whereas the variation degree for the electrical conductivity gradually reduces. At the  
360 same time, we also compared the presently obtained electrical conductivity results for  
361 anhydrous and hydrous gabbroic melts with other three representative calc-alkaline  
362 igneous melts reported by Ni et al. (2011), Laumonier et al. (2015) and Guo et al.  
363 (2017), as detailedly illustrated in Fig. 8. On the base of the previously calculating  
364 method for the degree of depolymerization (NBO/T) of melt transforming the detailed  
365 EPMA data, the magnitudes in the degree of depolymerization for our present  
366 gabbroic melt and other three representative calc-alkaline igneous rock melts (i.e.  
367 dacitic melt, andesitic melt and basaltic melt) are 0.65, 0.07, 0.35 and 0.81,  
368 respectively. As a whole, the electrical conductivity of four typical calc-alkaline  
369 igneous rock melts will increase with the rise of the degree of depolymerization at a  
370 fixed water content. As the water content will be enhanced from 0 to 8.32 wt%, the

371 electrical conductivity of each calc–alkaline igneous rock melts will dramatically  
372 increase. It is obviously observed that the correspondent variations in the electrical  
373 conductivity of calc–alkaline igneous rock melts along the orders from dacitic melt to  
374 andesitic melt to gabbroic melt to basaltic melt tend to gradually reduce, and become  
375 more and more convergent, accordingly. To my best knowledge, the magnitude in the  
376 degree of depolymerization (NBO/T) for the melt sample is highly positive relation  
377 with the content variations of alkali–bearing and alkali earth–bearing cations (i.e. Na<sup>+</sup>,  
378 K<sup>+</sup>, Ca<sup>2+</sup>, Mg<sup>2+</sup>, etc.) (Mysen et al., 1982; Lee et al., 2003; Di Genova et al., 2015).  
379 Just as presented the EPMA results, the total contents of alkali cations and alkali–  
380 earth cations are determined as the 11.54 wt% of dacitic melt reported by Laumonier  
381 et al. (2015), the 20.41 wt% of andesitic melt reported by Guo et al. (2017), the 30.23  
382 wt% of basaltic melt reported by Ni et al. (2011), and as well as the 25.53 wt% of  
383 gabbroic melt in this study. And thus, the degree of depolymerization for the calc–  
384 alkaline igneous rock melts along the orders from dacitic melt to andesitic melt to  
385 gabbroic melt to basaltic melt will gradually increase, accordingly. On the other hand,  
386 previous electrical conductivity results have confirmed that the main charge carriers  
387 of the calc–alkaline igneous melts are alkali cations and alkali–earth cations at high  
388 temperature and high pressure (Ni et al., 2011; Laumonier et al., 2015; Guo et al.,  
389 2017; Chen et al., 2018). And thus, the influence of the degree of depolymerization on  
390 the electrical conductivity of melt is possibly caused from the concentration of the  
391 alkali cations and alkali–earth cations. Accordingly, the electrical conductivity of  
392 calc–alkaline igneous melts will gradually increase with the rise of alkali cations and

393 alkali–earth cations along the orders from dacitic melt to andesitic melt to gabbroic  
394 melt to basaltic melt. In sum, as followed the orders from dacitic melt to andesitic  
395 melt to gabbroic melt to basaltic melt, it is very reasonable that the electrical  
396 conductivity of calc–alkaline igneous melts will be gradually enhanced with the rise  
397 of degree of depolymerization (NBO/T) under conditions of 1373 K and 1.0 GPa.

## 398 **5 Geophysical implications**

399 As a typical active plate geotectonic boundary, previously available  
400 magnetotelluric results have already revealed that the phenomenon of high  
401 conductivity anomalies is widespread distributed in the region of mid–ocean ridge  
402 (Key et al., 2013; Miensopust et al., 2014). For the representative Mohns ridge of the  
403 Arctic Ocean, there widely exist a large number of high conductive layers with their  
404 conductivity magnitude within the range of  $\sim 0.08\text{--}0.32\text{ S m}^{-1}$  at the correspondent  
405 depths from 4 km to 7 km (Johansen et al., 2019). All of these acquired seismic and  
406 gravitational survey datasets have confirmed that various volume percentages of  
407 gabbroic melt widely outcropped in the Mohns ridge of the Arctic Ocean at the depths  
408 of  $\sim 4\text{--}11$  km (Géli et al., 1994; Conley and Dunn, 2011). And therefore, the high  
409 conductivity anomalies in the Mohns ridge of the Arctic Ocean are possibly correlated  
410 with the gabbroic melt at high temperature and high pressure. In conjunction with our  
411 presently obtained experimental results on the electrical conductivity of anhydrous  
412 and hydrous gabbroic melts at conditions of 873–1373 K and 1.0–3.0 GPa, the typical  
413 Hashin–Shtrikman upper bound model and previously available magnetotelluric  
414 results, the electrical conductivity of gabbroic melt–olivine system was constructed in

415 detail, as displayed in Fig. 9. All of these influential ingredients including water  
 416 content and volume percentage were comprehensively considered. During the process  
 417 of the expansion of mid-ocean ridge caused by the rapid upwelling of asthenosphere  
 418 mantle, the geothermal distribution exhibited an abnormal behavior in the Mohns  
 419 ridge of the Arctic Ocean. As pointed out by Johansen et al. (2019), the temperature  
 420 on the top gabbro layer is approximate to 1373 K along the ultraslow-spreading  
 421 Arctic mid-ocean Mohns ridge region. In addition, the effect of pressure on the  
 422 electrical conductivity of gabbroic melt is rather feeble, and it can be neglected.

423 For the representative Mohns ridge of the Arctic Ocean, previously available  
 424 petrological and geochemical results have already revealed that the range of water  
 425 content for the crustal rock and melt in the Mohns ridge is ~0.25–2.64 wt% (Neumann  
 426 and Schilling, 1984; Poreda et al., 1986). The electrical conductivity results of  
 427 gabbroic melt with two different water contents (anhydrous and a water content of  
 428 2.59 wt%) are selected from our present studies. The electrical conductivity of olivine  
 429 at 1373 K and 1.0 GPa is properly extrapolated from the available experimental data  
 430 of polycrystalline olivine under conditions of 160 ppm wt water content, 873–1273 K  
 431 and 4.0–10.0 GPa reported by Dai and Karato (2014b). On the variation of volume  
 432 percentage for the gabbroic melt, the electrical conductivity of a gabbroic melt–  
 433 olivine system ( $\sigma_{HS+}$ ) can be expressed as (Hashin and Shtrikman, 1962),

$$434 \quad \sigma_{HS+} = \sigma_{melt} + [(1-X_{melt}) \cdot (\sigma_{olivine} - \sigma_{melt})^{-1} + X_{melt} / (3 \cdot \sigma_{melt})]^{-1} \quad (7)$$

435 In here, the signals of  $\sigma_{melt}$  and  $\sigma_{olivine}$  stand for the electrical conductivity of gabbroic  
 436 melt from the present study and that of polycrystalline olivine with a certain water

437 content of 160 ppm wt from Dai and Karato (2014b), respectively;  $X_{\text{melt}}$  stands for the  
438 volume percentage of gabbroic melt.

439 The electrical conductivity of gabbroic melt–olivine system with different  
440 volume percentage of gabbroic melt was successfully worked out at 1373 K and 1.0  
441 GPa, as displayed in Fig. 9. For the gabbroic melt–olivine system with a certain  
442 volume percentage of gabbroic melt, the electrical conductivity increases with the rise  
443 of water content in gabbroic melt. As far as the gabbroic melt containing a fixed water  
444 content, the electrical conductivity of gabbroic melt–olivine system gradually  
445 enhances as the volume percentage of gabbroic melt increases. As pointed out by  
446 Johansen et al. (2019), the range of electrical conductivity for the HCL in the Mohns  
447 ridge is  $\sim 0.08\text{--}0.32 \text{ S m}^{-1}$ , as displayed in the orange region of Fig. 9. For the  
448 anhydrous gabbroic melt, the required volume percentage for the high conductivity  
449 anomalies the ultraslow-spreading Arctic mid-ocean Mohns ridge region falls within  
450 the range of  $\sim 2.93\text{--}34.69 \text{ vol}\%$ , which is in good agreement with previously inferred  
451 results from geophysical observations (Géli et al., 1994; Conley and Dunn, 2011).  
452 When the water content of gabbroic melt increases, the required volume percentage  
453 for the HCL reduces accordingly. As for the gabbroic melt with a relatively high water  
454 content of 2.59 wt%, its volume percentage range of  $\sim 2.63\text{--}23.63 \text{ vol}\%$  is enough to  
455 explain the high conductivity anomalies. In summary, the high conductivity anomalies  
456 in the Mohns ridge of the Arctic Ocean could be interpreted by the anhydrous and  
457 hydrous gabbroic melt, and our present electrical conductivity results for gabbroic  
458 melt with different water contents can provide an important constraint for the water

459 content and volume percentage of gabbroic melt at depth range of ~4–7 km within the  
460 Mohns ridge region of the Arctic Ocean.

## 461 **Conclusions**

462 In the present studies, the electrical conductivity of gabbroic melt with different  
463 water contents of 0–8.32 wt% were measured at temperatures of 873–1373 K and  
464 pressures of 1.0–3.0 GPa. For the gabbroic melt with a fixed water content of 2.59  
465 wt%, the electrical conductivity of the sample decreases slightly with the rise of  
466 pressure, and its corresponding activation energy and activation volume are  
467 determined as  $0.87 \pm 0.04$  eV and  $-1.98 \pm 0.02$  cm<sup>3</sup> mole<sup>-1</sup>, respectively. When water  
468 content of gabbroic melt enhances from 0 to 8.32 wt% under the certain conditions of  
469 873–1373 K and 1.0 GPa, the electrical conductivity of gabbroic melts tends to visibly  
470 increase, and whereas the activation enthalpy gradually reduces from 0.93 eV to 0.63  
471 eV, accordingly. Furthermore, the functional relation models for the electrical  
472 conductivity of gabbroic melt with the variations of temperature, pressure and water  
473 content are constructed at high–temperature and high–pressure conditions,  
474 respectively. By virtue of typical Hashin–Shtrikman upper bound model, the electrical  
475 conductivity of gabbroic melt–olivine system on the variation of melt volume  
476 percentage is calculated under the conditions of four different water contents of  
477 gabbroic melt (i.e. 0, 2.59 wt%, 5.92 wt% and 8.32 wt%), 1373 K and 1.0 GPa, which  
478 can be employed to reasonably explain the high conductivity anomalies in the Mohns  
479 ridge of the Arctic Ocean observed by the previously available field MT results.

480 *Data availability.* The data that support the findings of this study are available  
481 from the first author upon reasonable request.

482 *Acknowledgements.* This research was financially supported by the NSF of China  
483 (grant number 42072055 and 42274137) and the Youth Innovation Promotion  
484 Association of CAS (grant number 2019390).

485 *Declaration of competing interest.* The authors declare that they have no  
486 conflict of interest.



487 **References**

- 488 Almeev, R., Holtz, F., Koepke, J., Haase, K., and Devey, C.: Depths of partial  
489 crystallization of H<sub>2</sub>O-bearing MORB: Phase equilibria simulations of basalts at  
490 the MAR near Ascension Island (7–11°S), *J. Petrol.*, 49, 25–45, 2008.
- 491 Chen, J. Y., Gaillard, F., Villaros, A., Yang, X. S., Laumonier, M., Jolivet, L.,  
492 Unsworth, M., Hashim, L., Scaillet, B., and Richard, G.: Melting conditions in  
493 the modern Tibetan crust since the Miocene, *Nat. Commun.*, 9, 3515,  
494 <https://doi.org/10.1038/s41467-018-05934-7>, 2018.
- 495 Conley, M. M. and Dunn, R. A.: Seismic shear wave structure of the uppermost  
496 mantle beneath the Mohns Ridge, *Geochem. Geophys. Geosyst.*, 12, Q0AK01,  
497 <https://doi.org/10.1029/2011GC003792>, 2011.
- 498 Dai, L. D., Li, H. P., Hu, H. Y., and Shan, S. M.: Experimental study of grain  
499 boundary electrical conductivities of dry synthetic peridotite under  
500 high-temperature, high-pressure, and different oxygen fugacity conditions, *J.*  
501 *Geophys. Res. Solid Earth*, 113, B12211, <https://doi.org/10.1029/2008JB005820>,  
502 2008.
- 503 Dai, L. D. and Karato, S. I.: Electrical conductivity of pyrope-rich garnet at high  
504 temperature and high pressure, *Phys. Earth Planet. Inter.*, 176, 83–88, 2009a.
- 505 Dai, L. D. and Karato, S. I.: Electrical conductivity of orthopyroxene: Implications for  
506 the water content of the asthenosphere, *Proc. Jpn. Acad. Ser. B*, 85, 466–475,  
507 2009b.
- 508 Dai, L. D. and Karato, S. I.: Electrical conductivity of wadsleyite at high temperatures

509 and high pressures, *Earth Planet. Sci. Lett.*, 287, 277–283, 2009c.

510 Dai, L. D., Li, H. P., Hu, H. Y., Shan, S. M., Jiang, J. J., and Hui, K. S.: The effect of  
511 chemical composition and oxygen fugacity on the electrical conductivity of dry  
512 and hydrous garnet at high temperatures and pressures, *Contrib. Mineral. Petrol.*,  
513 163, 689–700, 2012.

514 Dai, L. D., Li, H. P., Hu, H. Y., Jiang, J. J., Hui, K. S., and Shan, S. M.: Electrical  
515 conductivity of  $\text{Alm}_{82}\text{Py}_{15}\text{Grs}_3$  almandine-rich garnet determined by impedance  
516 spectroscopy at high temperatures and high pressures, *Tectonophysics*, 608,  
517 1086–1093, 2013.

518 Dai, L. D., Hu, H. Y., Li, H. P., Jiang, J. J., and Hui, K. S.: Effects of temperature,  
519 pressure and chemical composition on the electrical conductivity of granite and  
520 its geophysical implications, *Am. Mineral.*, 99, 1420–1428, 2014.

521 Dai, L. D. and Karato, S. I.: Influence of oxygen fugacity on the electrical  
522 conductivity of olivine under hydrous conditions: Implications for the  
523 mechanism of conduction. *Phys. Earth Planet. Inter.*, 232, 57–60, 2014a.

524 Dai, L. D. and Karato, S. I.: The effect of pressure on the electrical conductivity of  
525 olivine under the hydrogen-rich conditions, *Phys. Earth Planet. Inter.*, 232, 51–56,  
526 2014b.

527 Dai, L. D., Hu, H. Y., Li, H. P., Hui, K. S., Jiang, J. J., Li, J., and Sun, W. Q.:  
528 Electrical conductivity of gabbro: The effects of temperature, pressure and  
529 oxygen fugacity, *Eur. J. Mineral.*, 27, 215–224, 2015.

530 Dai, L. D., Hu, H. Y., Li, H. P., Wu, L., Hui, K. S., Jiang J. J., and Sun, W. Q.:

531 Influence of temperature, pressure, and oxygen fugacity on the electrical  
532 conductivity of dry eclogite, and geophysical implications, *Geochem. Geophys.*  
533 *Geosyst.*, 17, 2394–2407, 2016.

534 Dai, L. D. and Karato, S. I.: Electrical conductivity of Ti-bearing hydrous olivine  
535 aggregates at high temperature and high pressure, *J. Geophys. Res. Solid Earth*,  
536 125, e2020JB020309, <https://doi.org/10.1029/2020JB020309>, 2020.

537 Di Genova, D., Morgavi, D., Hess, K. U., Neuville, D. R., Borovkov, N., Perugini, D.,  
538 and Dingwell, D. B.: Approximate chemical analysis of volcanic glasses using  
539 Raman spectroscopy, *J. Raman Spectrosc.*, 46, 1235–1244, 2015.

540 Dixon, J. B., Stolper, E. M., and Holloway, J. R.: An experimental study of water and  
541 carbon dioxide solubilities in mid-ocean ridge basaltic liquids. Part I: Calibration  
542 and solubility models, *J. Petrol.*, 36, 1607–1631, 1995.

543 Förster, M. W. and Selway, K.: Melting of subducted sediments reconciles  
544 geophysical images of subduction zones, *Nat. Commun.*, 12, 1320,  
545 <https://doi.org/10.1038/s41467-021-21657-8>, 2021.

546 Géli, L., Renard, V., and Rommevaux, C.: Ocean crust formation processes at very  
547 slow spreading centers: A model for the Mohns Ridge, near 72°N, based on  
548 magnetic, gravity, and seismic data, *J. Geophys. Res. Solid Earth*, 99, 2995–3013,  
549 1994.

550 Guo, X., Li, B., Ni, H. W., and Mao, Z.: Electrical conductivity of hydrous andesitic  
551 melts pertinent to subduction zones, *J. Geophys. Res. Solid Earth*, 122, 1777–  
552 1788, 2017.

553 Hashin, Z. and Shtrikman, S.: A variation approach to the theory of effective magnetic  
554 permeability of multiphase materials, *J. Appl. Phys.*, 33, 3125–3131, 1962.

555 Hong, M. L., Dai, L. D., Hu, H. Y., Yang, L. F. and Zhang, X. Y.: Pressure-induced  
556 structural phase transitions in natural kaolinite investigated by Raman  
557 spectroscopy and electrical conductivity, *Am. Mineral.*, 107, 385–394, 2022.

558 Hu, H. Y., Dai, L. D., Sun, W. Q., Wang, M. Q., and Jing, C. X.: Constraints on fluids  
559 in the continental crust from laboratory-based electrical conductivity  
560 measurements of plagioclase, *Gondwana Res.*, 107, 1–12, 2022a.

561 Hu, H. Y., Jing, C. X., Dai, L. D., Yin, C. Y. and Chen, D. M.: Electrical conductivity  
562 of siderite and its implication for high conductivity anomaly in the slab-mantle  
563 wedge interface, *Front. Earth Sci.*, 10, 985740,  
564 <https://doi.org/10.3389/feart.2022.985740>, 2022b.

565 Huang, X. G., Xu, Y. S., and Karato S. I.: Water content in the transition zone from  
566 electrical conductivity of wadsleyite and ringwoodite, *Nature*, 434, 746–749,  
567 2005.

568 Johansen, S. E., Panzner, M., Mittet, R., Amundsen, H. E. F., Lim, I., Vik, E., Landrø,  
569 M., and Arntsen, B.: Deep electrical imaging of the ultraslow-spreading Mohns  
570 ridge, *Nature*, 567, 379–383, 2019.

571 Key, K., Constable, S., Liu, L. J., and Pommier, A.: Electrical image of passive mantle  
572 upwelling beneath the northern East Pacific Rise, *Nature*, 495, 499–502, 2013.

573 Laumonier, M., Gaillard, F., and Sifre, D.: The effect of pressure and water  
574 concentration on the electrical conductivity of dacitic melts: Implication for

575 magnetotelluric imaging in subduction areas, *Chem. Geol.*, 418, 66–76, 2015.

576 Lee, S. K., Mysen, B. O., and Cody, G. D.: Chemical order in mixed-cation silicate  
577 glasses and melts, *Phys. Rev. B*, 68, 214206,  
578 <https://doi.org/10.1103/PhysRevB.68.214206>, 2003.

579 Leuthold, J., Lissenberg, C. J., O’Driscoll, B., Karakas, O., Falloon, T., Klimentyeva,  
580 D. N., and Ulmer, P.: Partial melting of lower oceanic crust gabbro: Constraints  
581 from poikilitic clinopyroxene primocrysts, *Front. Earth Sci.*, 6, 15,  
582 <https://doi.org/10.3389/feart.2018.00015>, 2018.

583 Li, G. H., Gao, Y., Zhou, Y. Z., Ju, C. H., Shi, Y. T., and Cui, Q. H.: A low-velocity  
584 layer atop the mantle transition zone beneath the western Central Asian Orogenic  
585 Belt: Upper mantle melting induced by ancient slab subduction, *Earth Planet. Sci.  
586 Lett.*, 578, 117287, <https://doi.org/10.1016/j.epsl.2021.117287>, 2022.

587 Luhr, J. F.: Glass inclusions and melt volatile contents at Parícutin Volcano, Mexico,  
588 *Contrib. Mineral. Petrol.*, 142, 261–283, 2001.

589 Maumus, J., Bagdassarov, N., and Schmeling, H.: Electrical conductivity and partial  
590 melting of mafic rocks under pressure, *Geochim. Cosmochim. Ac.*, 69, 4703–  
591 4718, 2005.

592 Miensoopust, M. P., Jones, A. G., Hersir, G. P., and Vilhjálmsson, A. M.: The  
593 Eyjafjallajökull volcanic system, Iceland: Insights from electromagnetic  
594 measurements, *Geophys. J. Int.*, 199, 1187–1204, 2014.

595 Mysen, B. O., Virgo, D., and Seifert, F. A.: The structure of silicate melts:  
596 Implications for chemical and physical properties of natural magma, *Rev.*

597 Geophys., 20, 353–383, 1982.

598 Neumann, E. R. and Schilling, J. G.: Petrology of basalts from the Mohns–Knipovich  
599 Ridge; the Norwegian–Greenland Sea, *Contrib. Mineral. Petrol.*, 85, 209–223,  
600 1984.

601 Ni, H. W., Keppler, H., and Behrens, H.: Electrical conductivity of hydrous basaltic  
602 melts: Implications for partial melting in the upper mantle, *Contrib. Mineral.  
603 Petrol.*, 162, 637–650, 2011.

604 Poreda, R., Schilling, J. G., and Craig, H.: Helium and hydrogen isotopes in ocean–  
605 ridge basalts north and south of Iceland, *Earth Planet. Sci. Lett.*, 78, 1–17, 1986.

606 Saito, S. and Bagdassarov, N. S: Laboratory measurements of electrical conductivity  
607 in a gabbro of the Oman ophiolite at high–pressures and high–temperatures:  
608 Implications for interpretation of resistivity structures of lower oceanic crust, *J.  
609 Mineral. Petrol. Sci.*, 113, 112–117, 2018.

610 Sato, H. and Ida, Y.: Low frequency electrical impedance of partially molten gabbro:  
611 the effect of melt geometry on electrical properties, *Tectonophysics*, 107, 105–  
612 134, 1984.

613 Schilling, F. R., Partzsch, G. M., Brasse, H., and Schwarz, G.: Partial melting below  
614 the magmatic arc in the central Andes deduced from geoelectromagnetic field  
615 experiments and laboratory data, *Phys. Earth Planet. Inter.*, 103, 17–31, 1997.

616 Shaw, A. M., Behn, M. D., Humphris, S. E., Sohn, R. A., and Gregg, P. M.: Deep  
617 pooling of low degree melts and volatile fluxes at the 85°E segment of the  
618 Gakkel Ridge: Evidence from olivine-hosted melt inclusions and glasses, *Earth*

619 Planet. Sci. Lett., 289, 311–322, 2010.

620 Shen, Y. and Forsyth, D. W.: Geochemical constraints on initial and final depths of  
621 melting beneath mid-ocean ridges, *J. Geophys. Res. Solid Earth*, 100, 2211–2237,  
622 1995.

623 Sim, S. J., Spiegelman, M., Stegman, D. R., and Wilson, C.: The influence of  
624 spreading rate and permeability on melt focusing beneath mid-ocean ridges, *Phys.*  
625 *Earth Planet. Inter.*, 304, 106486, <https://doi.org/10.1016/j.pepi.2020.106486>,  
626 2020.

627 Stolper, E.: The speciation of water in silicate melts, *Geochim. Cosmochim. Ac.*, 46,  
628 2609–2620, 1982.

629 Turner, S. J. and Langmuir, C. H.: Sediment and ocean crust both melt at subduction  
630 zones, *Earth Planet. Sci. Lett.*, 584, 117424,  
631 <https://doi.org/10.1016/j.epsl.2022.117424>, 2022.

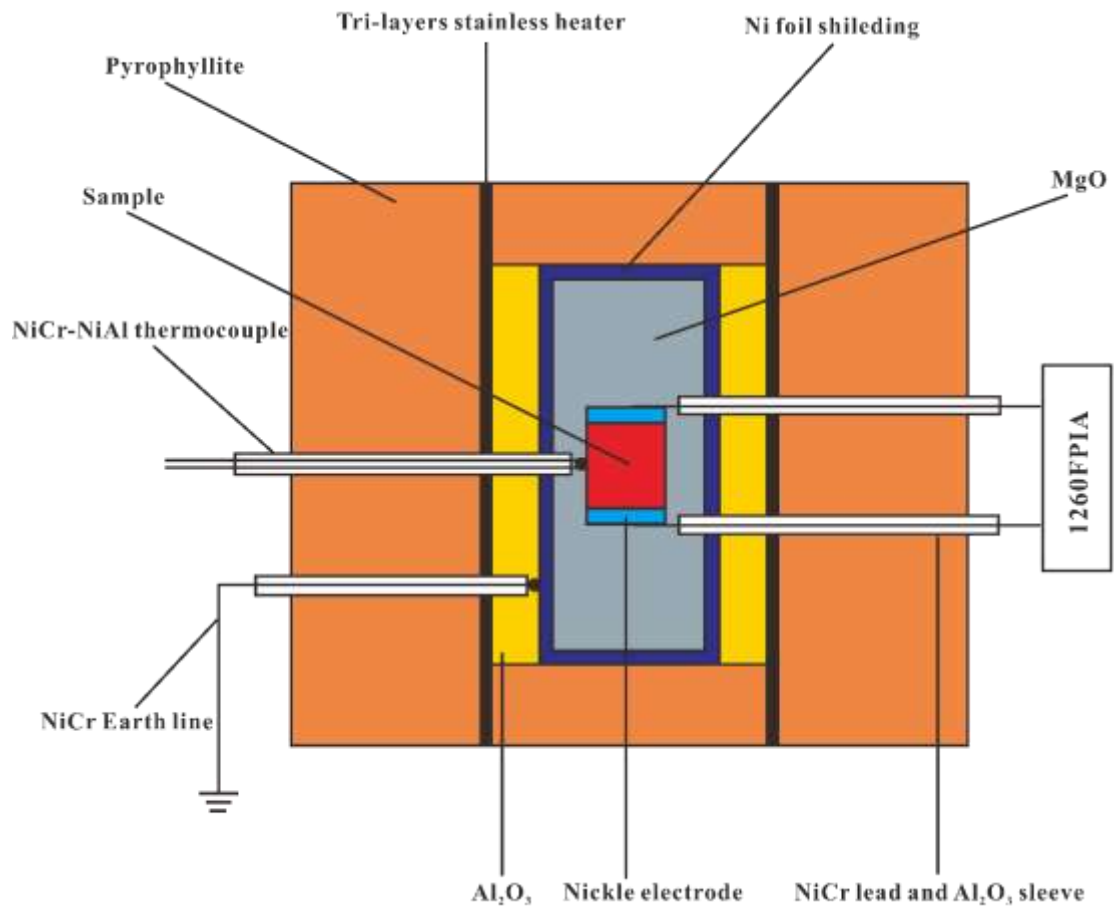
632 Tyburczy, J. A. and Roberts, J. J.: Low frequency electrical response of polycrystalline  
633 olivine compacts: Grain boundary transport, *Geophys. Res. Lett.*, 17, 1985–1988,  
634 1990.

635 Wallace, P. J.: Volatiles in subduction zone magmas: concentrations and fluxes based  
636 on melt inclusion and volcanic gas data, *J. Volcanol. Geoth. Res.*, 140, 217–240,  
637 2005.

638 White, R. S., Minshull, T.A., Bickle, M. J., and Robinson, C. J.: Melt generation at  
639 very slow-spreading oceanic ridges: Constraints from geochemical and  
640 geophysical data, *J. Petrol.*, 42, 1171–1196, 2001.

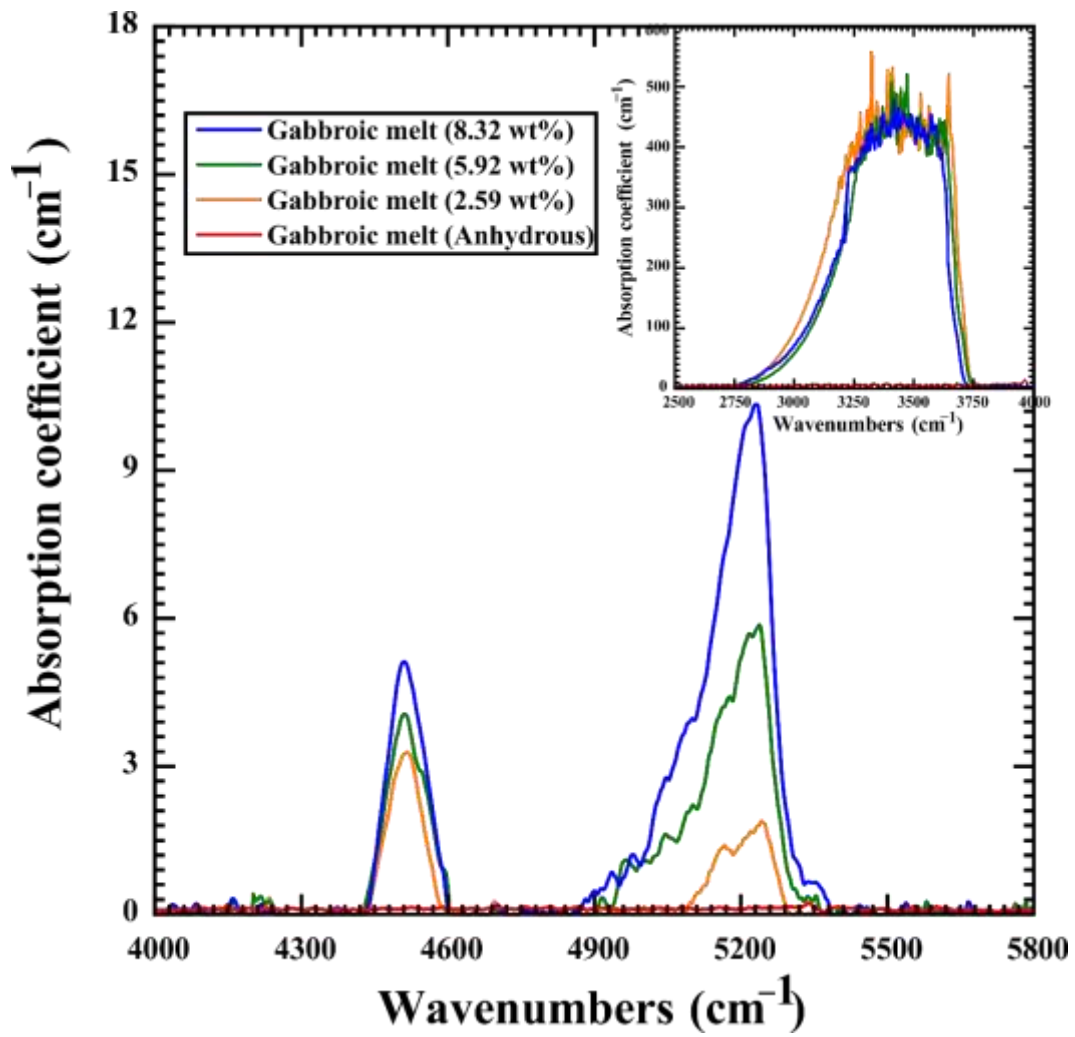
641 Wu, K., Ling, M. X., Hu, Y. B., Guo, J., Jiang, X. Y., Sun, S. J., Liang, H. Y., Liu, X.,  
642 and Sun, W. D.: Melt-fluxed melting of the heterogeneously mixed lower arc  
643 crust: A case study from the Qinling orogenic belt, Central China, *Geochem.*  
644 *Geophys. Geosyst.*, 19, 1767–1788, 2018.





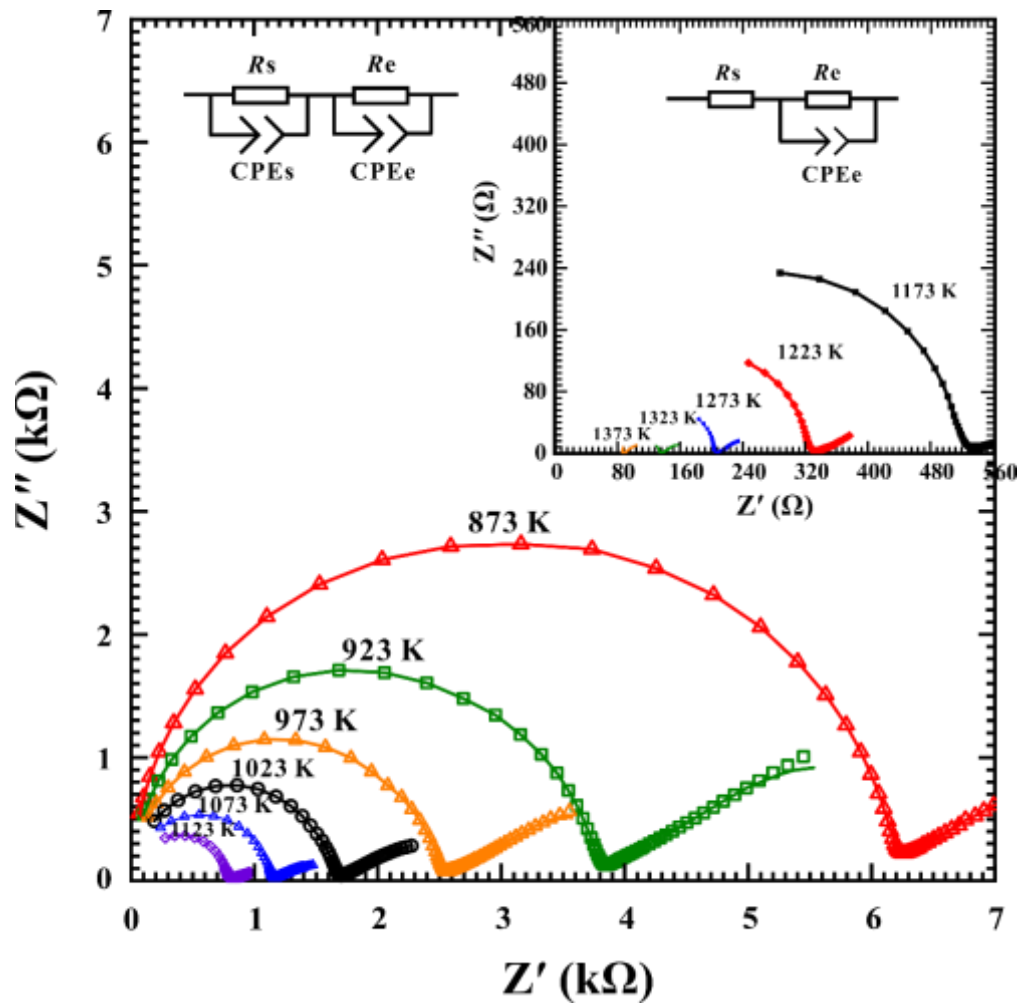
645

646 **Figure 1.** The experimental setup for the electrical conductivity measurements of  
 647 gabbroic melt at high temperatures and high pressures.



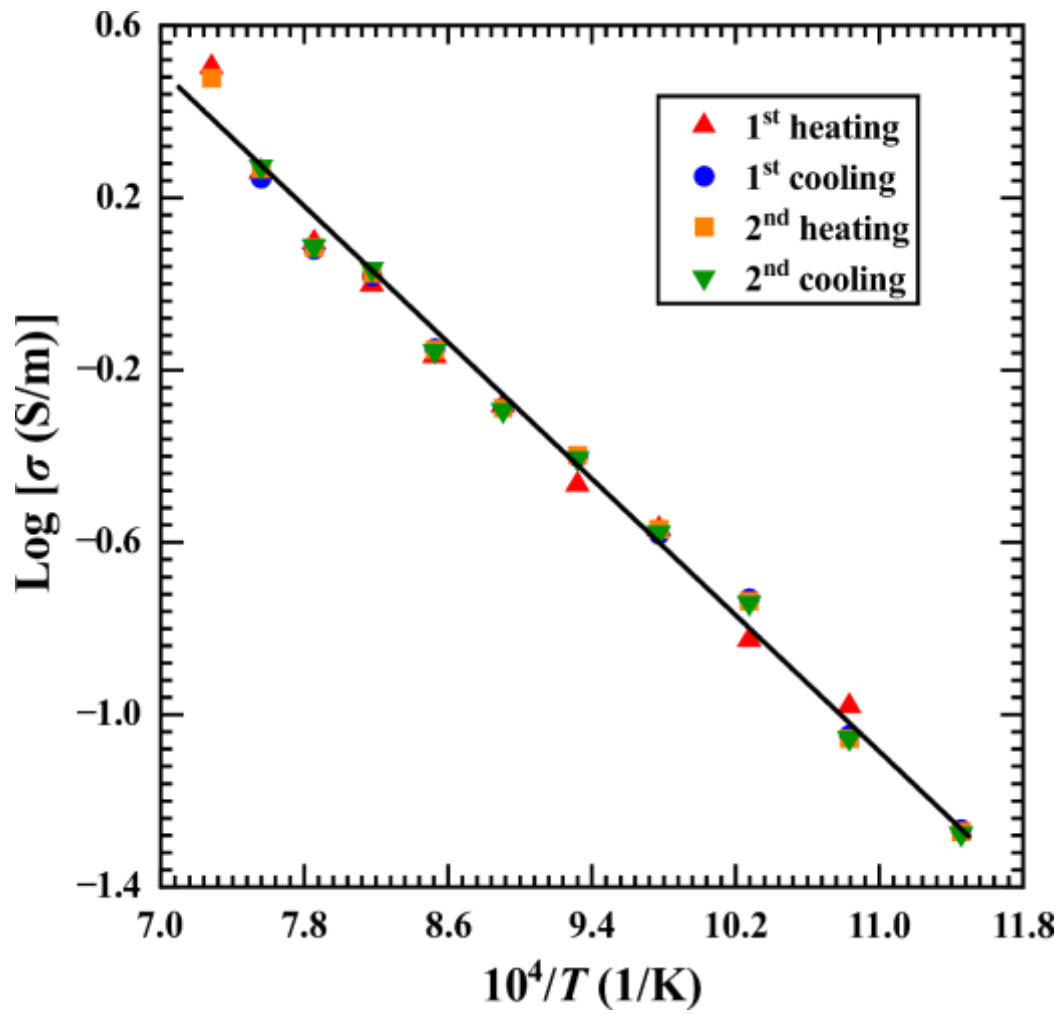
648

649 **Figure 2.** The representative FT-IR spectra of the gabbroic melt with various water  
 650 contents in the wavenumbers range of 4000–5800 cm<sup>-1</sup> and 2500–4000 cm<sup>-1</sup>.



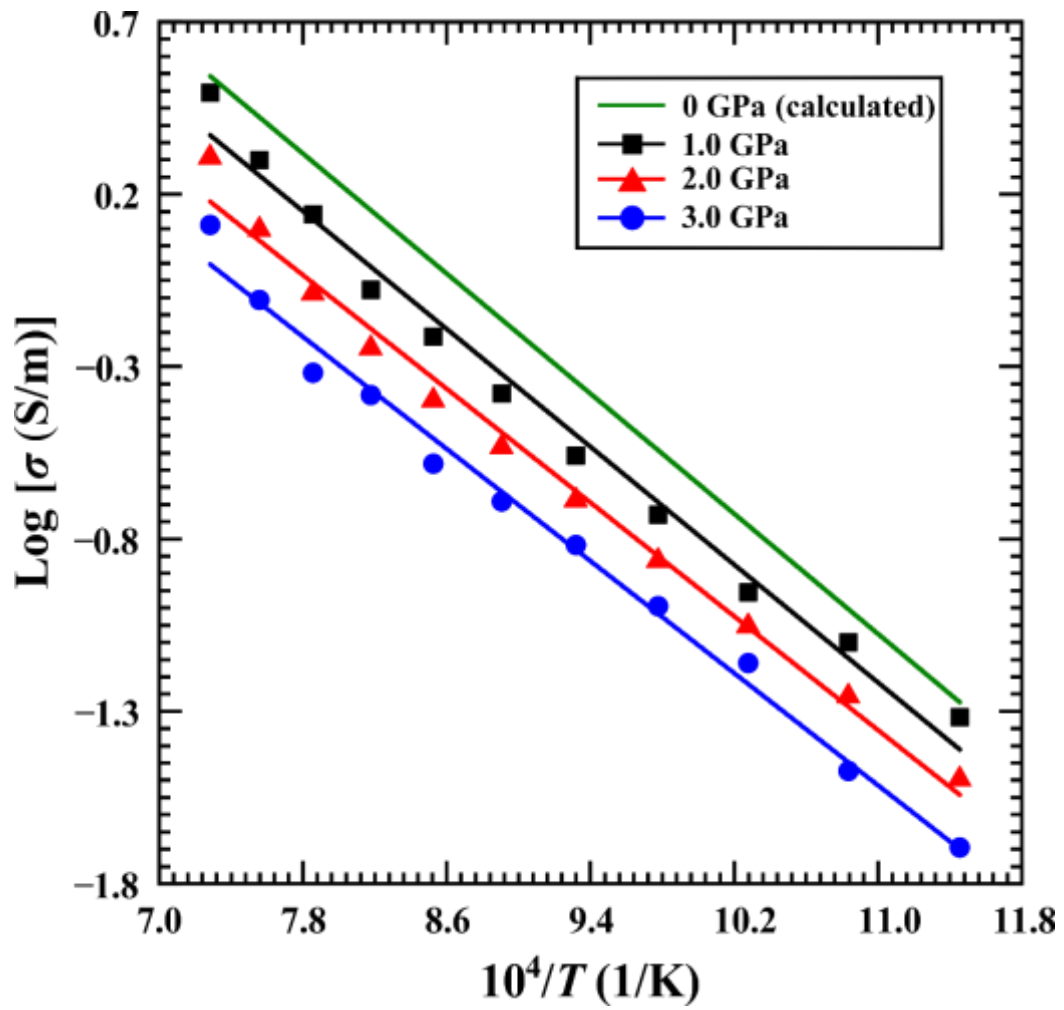
651

652 **Figure 3.** Typical complex impedance spectra for gabbroic melt (DW209) with a  
 653 fixed water content of 2.59 wt% at temperatures of 873–1373 K and pressure of 2.0  
 654 GPa in the frequency range from  $10^0$  Hz to  $10^6$  Hz. The fitting results for the  
 655 experimental data are displayed by using the solid line.



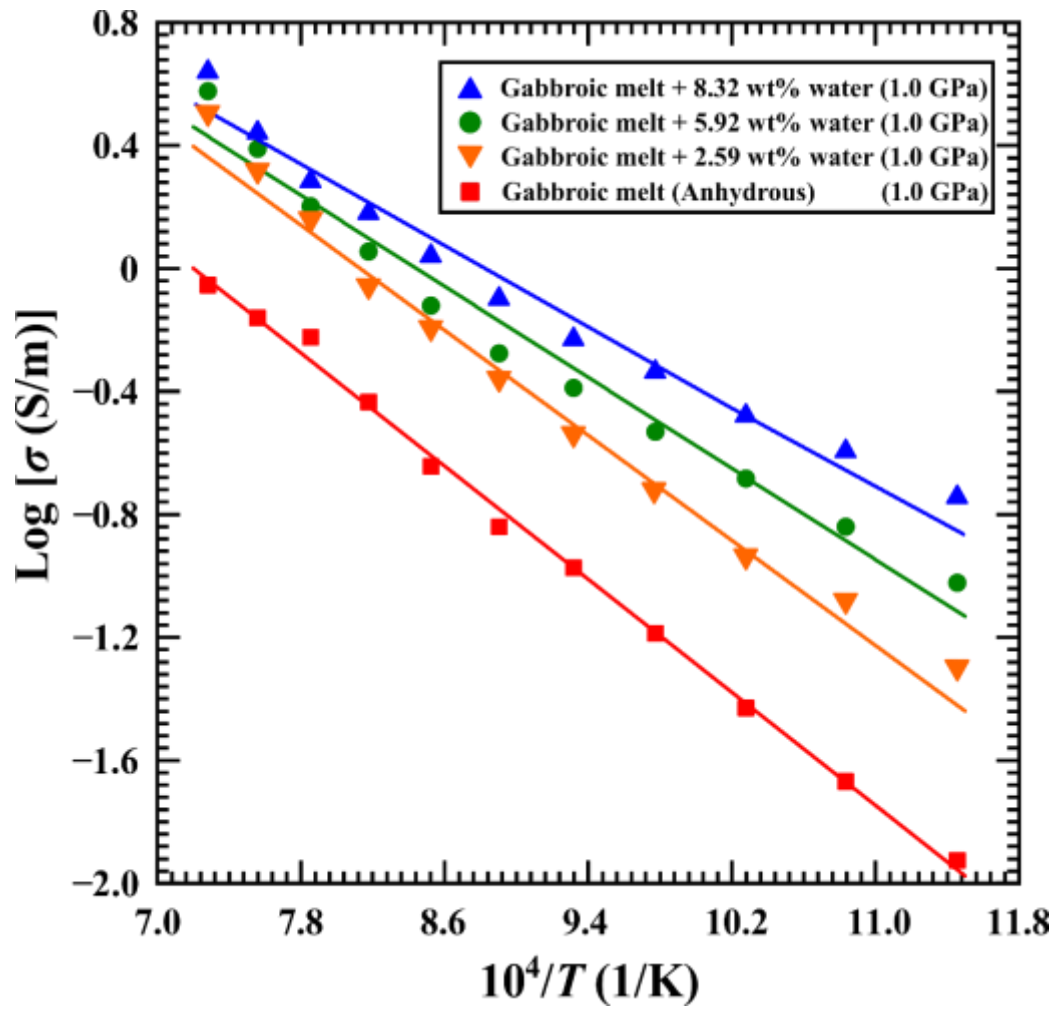
656

657 **Figure 4.** The electrical conductivity of gabbroic melt (DW212) with a fixed water  
 658 content of 2.59 wt% among two heating–cooling cycles at a pressure of 3.0 GPa.



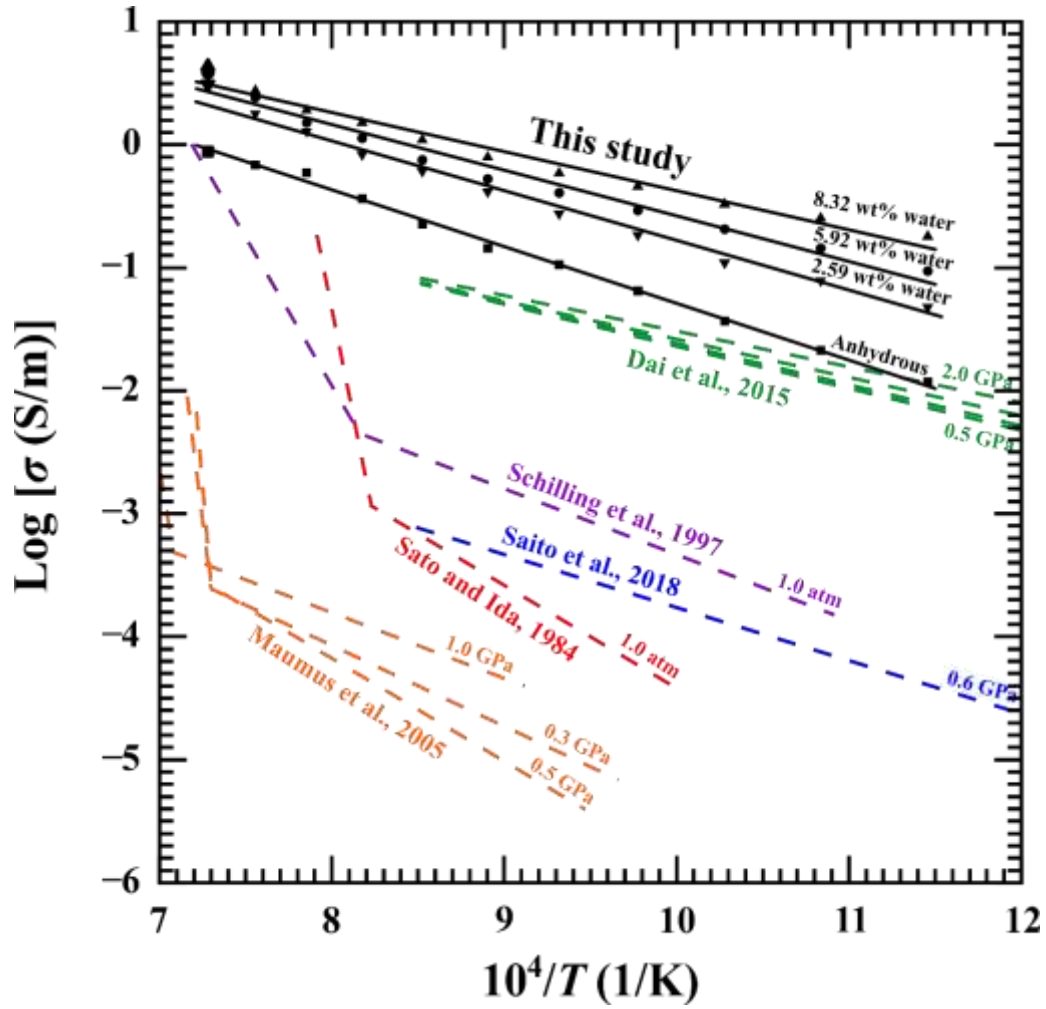
659

660 **Figure 5.** Influence of pressure on the electrical conductivity of gabbroic melt with a  
 661 fixed water content of 2.59 wt% at the temperature ranges of 873–1373 K.



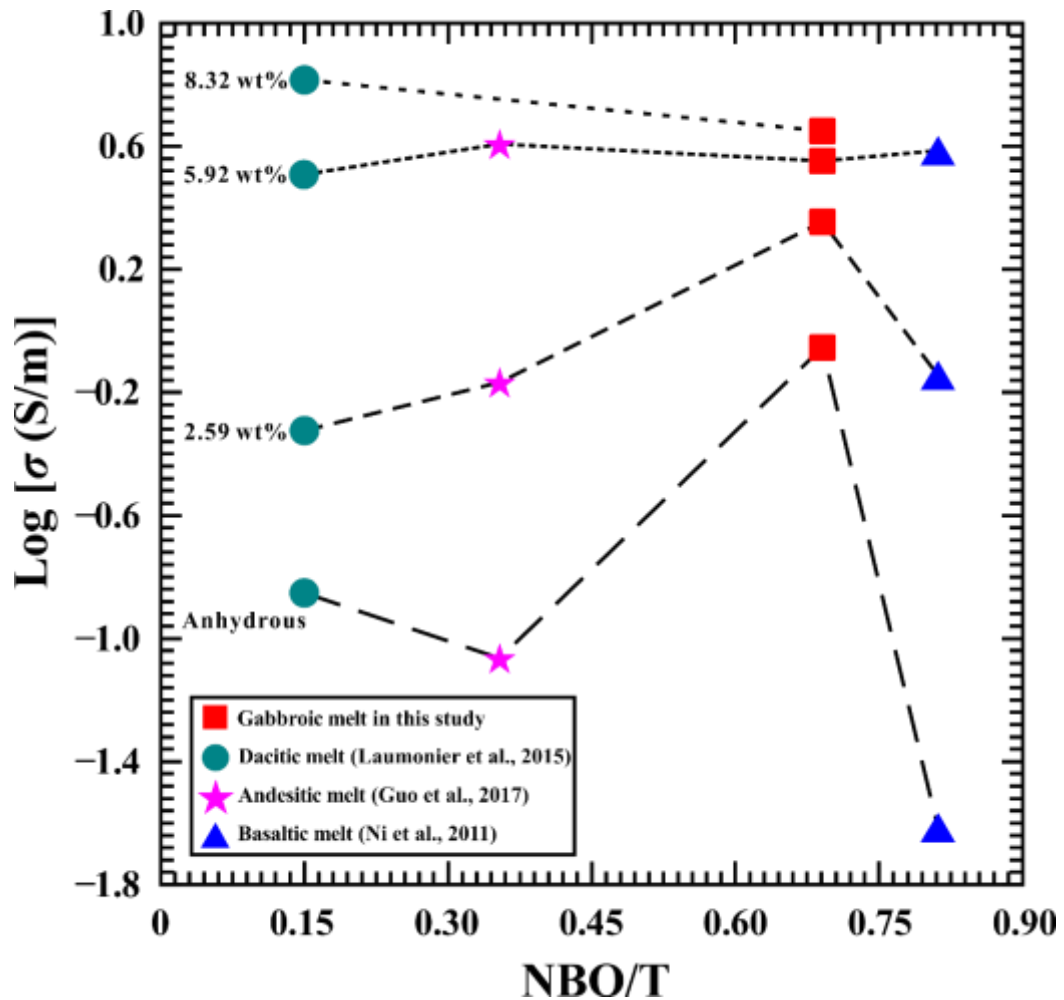
662

663 **Figure 6.** Logarithmic electrical conductivity of gabbroic melts with four different  
 664 water contents as a function of reciprocal temperature at conditions of 873–1373 K  
 665 and 1.0 GPa.



666

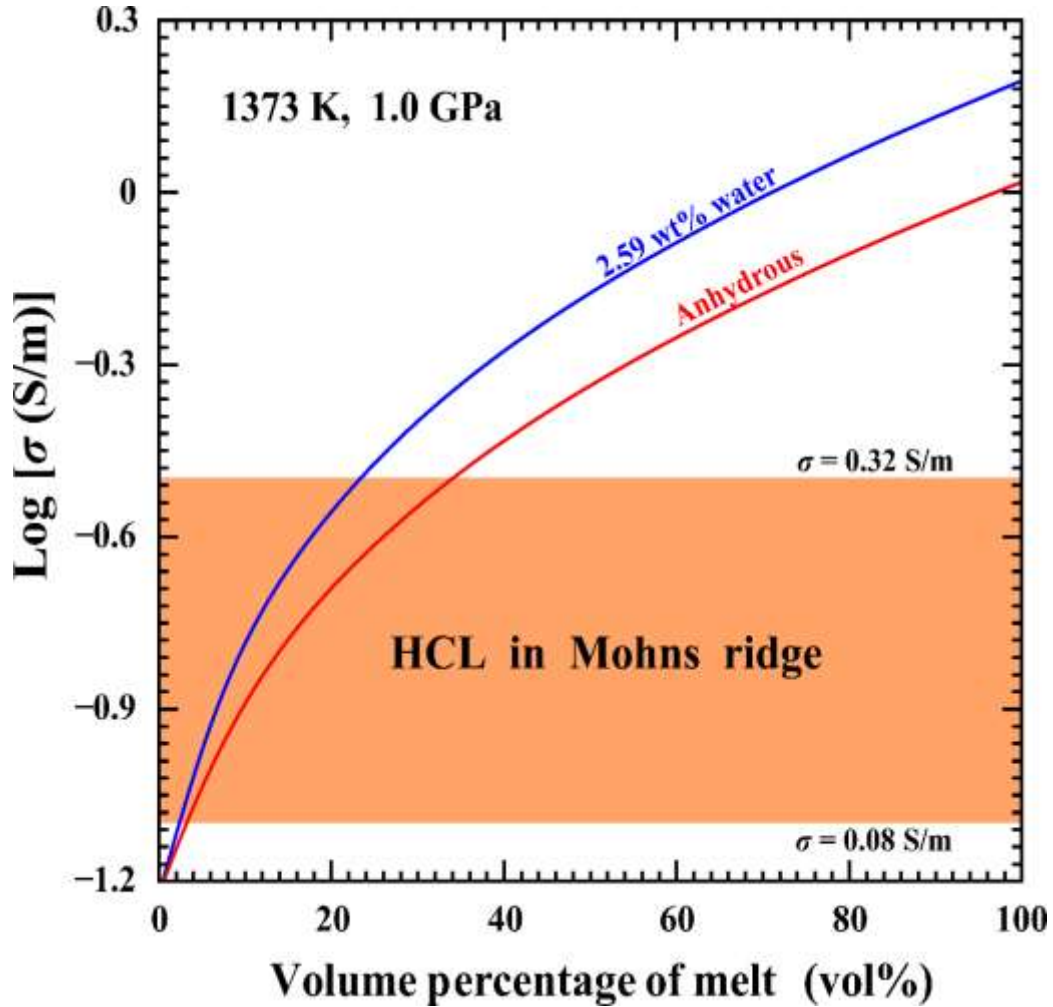
667 **Figure 7.** Comparison of electrical conductivity of gabbroic melts with the previously  
 668 reported results from five natural gabbro samples at high-temperature and high-  
 669 pressure conditions.



670

671 **Figure 8.** Variation of electrical conductivity of gabbroic melt and three  
 672 representative calc-alkaline igneous rock melts with the degree of depolymerization  
 673 (NBO/T) under conditions of four different water contents (i.e. 0, 2.59 wt%, 5.92 wt%  
 674 and 8.32 wt%), 1373 K and 1.0 GPa. Data source: basaltic melt from Ni et al. (2011),  
 675 andesitic melt from Guo et al. (2017), and dacitic melt from Laumonier et al. (2015).





676

677 **Figure 9.** The electrical conductivity for the gabbroic melt–olivine system at  
 678 temperature of 1373 K and 1.0 GPa, calculated with Eq. 7 of the Hashin–  
 679 Shtrikman upper bound model. The electrical conductivity of olivine from Dai  
 680 and Karato (2014b) was adopted as  $\sigma_{\text{olivine}}$ . The orange region indicates the  
 681 gabbro layer within the electrical conductivity range of 0.08–0.32 S m<sup>-1</sup> along  
 682 the ultraslow–spreading Arctic mid–ocean Mohns ridge region (Johansen et al.,  
 683 2019).

684 **Table 1.** The chemical composition of the gabbroic melts by virtue of the electronic  
 685 probe microscopy analysis (EPMA).

Sample	SiO <sub>2</sub>	TiO <sub>2</sub>	Al <sub>2</sub> O <sub>3</sub>	FeO	MnO	MgO	CaO	Na <sub>2</sub> O	K <sub>2</sub> O	Total (wt%)	NBO/T
Gabbroic melt (anhydrous)	51.32	0.56	12.37	9.93	0.20	11.06	11.82	2.15	0.50	99.91	0.6911
Gabbroic melt (2.59 wt% water)	51.22	0.55	12.40	9.92	0.18	11.29	11.72	2.19	0.48	99.95	0.6854
Gabbroic melt (5.92 wt% water)	51.23	0.57	12.40	9.87	0.18	11.28	11.70	2.21	0.47	99.91	0.6869
Gabbroic melt (8.32 wt% water)	51.22	0.57	12.40	9.88	0.17	11.27	11.69	2.21	0.46	99.86	0.6938

686

687 **Table 2.** Fitted parameters of Arrhenius relation for the electrical conductivity of  
 688 hydrous and anhydrous gabbroic melts under conditions of 873–1373 K and 1.0–3.0  
 689 GPa.

Sample	$T$ (K)	$P$ (GPa)	Water content	Water content	Log $\sigma_0$ ( $\sigma_0$ in S m <sup>-1</sup> )	$\Delta H$ (eV)
			Before experiment (wt%)	After experiment (wt%)		
DW201	873–1373	1.0	8.32 ± 0.02	8.30 ± 0.01	2.80 ± 0.16	0.63 ± 0.03
DW204	873–1373	1.0	5.92 ± 0.01	5.90 ± 0.02	3.13 ± 0.18	0.74 ± 0.04
DW208	873–1373	1.0	2.59 ± 0.01	2.57 ± 0.01	3.48 ± 0.15	0.85 ± 0.03
DW209	873–1373	2.0	2.59 ± 0.03	2.58 ± 0.01	3.18 ± 0.13	0.83 ± 0.03
DW212	873–1373	3.0	2.59 ± 0.01	2.50 ± 0.02	2.79 ± 0.11	0.81 ± 0.03
DW210	873–1373	1.0	0	0	3.31 ± 0.08	0.93 ± 0.02

690

691 **Table 3.** Parameter values for the electrical conductivity of gabbroic melt with water  
692 content of 2.59 wt% at pressures of 1.0–3.0 GPa. The equation  $\sigma = \sigma_0 \cdot \exp(-\frac{\Delta U + P\Delta V}{kT})$   
693 is adopted for the globally fitting of electrical conductivity data. In consideration of  
694 a strong dependence of the pre-exponential factor ( $\sigma_0$ ) on the pressure, we used the  
695 relation  $\sigma_0 = A_0 \cdot (1 - BP)$ .

$\sigma_0$ (S m <sup>-1</sup> )	$B$ (GPa <sup>-1</sup> )	$\Delta U$ (eV)	$\Delta V$ (cm <sup>3</sup> mole <sup>-1</sup> )
$A_0 = 2623.27 \pm 1.41$	$B = 0.22 \pm 0.03$	$0.87 \pm 0.04$	$-1.98 \pm 0.52$

696

697 **Table 4.** Parameter values for the electrical conductivity of gabbroic melts with  
 698 different water contents under conditions of 873–1373 K and 1.0 GPa. The  
 699 equation  $\sigma = (A_1 + A_2 \cdot C_w^r) \cdot \exp\left(\frac{-\Delta H_0 - \alpha C_w^\beta}{RT}\right)$  is adopted for the globally fitting of electrical  
 700 conductivity data.

$A_1$ (S m <sup>-1</sup> )	$A_2$ (S m <sup>-1</sup> )	$\Delta H_0$ (eV)	$\alpha$	$\beta$	$r$
6760±234	66069±240	1.03±0.04	34.85±2.24	17.70±1.31	0.43±0.05

701